Materials Horizons

ROYAL SOCIETY OF CHEMISTRY

COMMUNICATION

View Article Online
View Journal

Cite this: DOI: 10.1039/d5mh00082c

Received 15th January 2025,
Accepted 22nd April 2025

DOI: 10.1039/d5mh00082c

rsc.li/materials-horizons

Spiropyran-based glutamate nanovalve for neuronal stimulation†

M. Blanco-Formoso,‡[ab] F. Galluzzi,‡[cd] F. Vacca,‡[ce] T. Gianiorio,[cf] I. Piergentili,[g] A. B. Cook,[g] P. L. W. Welzen,[g] J. C. M. van Hest,[g] S. Di Marco,[ce] F. Tantussi,[a] F. Benfenati,[ce] E. Colombo‡*[ce] and F. De Angelis‡*[a]

One of the main challenges in medical applications is achieving precise spatial and temporal control over the release of active molecules, such as neurotransmitters. To address this issue, we engineered a nanovalve that can deliver active molecules on demand by activating or deactivating a light-sensitive chemical barrier. This valve is composed of a polymer containing a spiropyran moiety, which can switch from a hydrophobic to a hydrophilic state upon photo-stimulation. Accordingly, the nanovalve either blocks or allows molecular diffusion through a solid-state nanopore array. Here, we demonstrate that the system blocks up to 96% of the translocation of the neurotransmitter glutamate and that the on-demand release of glutamate upon light stimulation reaches 60 μM h^{-1}, mimicking a physiological synaptic release rate. We proved its cytocompatibility and analyzed its potential for the stimulation of primary neurons and blind retinal explants by patch-clamp experiments. These results represent a milestone for the development of biomimetic neuroprostheses restoring chemical synaptic transmission lost by degeneration or delivering drugs in a light-controlled fashion.

New concepts

Neural stimulation is one of the few therapeutic options for a number of central nervous system pathologies. State-of-the-art methodologies for the modulation of neural activity hardly foresee a naturalistic recovery of the lost brain functions. Biomimetic strategies exploiting the inherent properties of synaptic transmission represent a breakthrough in neuronal stimulation technologies. Here, we engineered a nanovalve that provides denervated or injured neurons with an on-demand delivery of glutamate by activating or deactivating a photosensitive chemical barrier upon illumination with high spatial resolution, mimicking the release of neurotransmitter from the active zones of axon terminals in neurons. The device is composed of a solid-state array of nanopores covered by a polymeric layer containing a spiropyran moiety, which can switch from hydrophobic to hydrophilic configuration upon photo-stimulation, thereby blocking or releasing the neurotransmitter. We characterized the switching dynamics of the nanovalve, proved its biocompatibility and analyzed its potential for the stimulation of primary neurons and blind retinal explants by patch-clamp experiments upon illumination. These results represent a milestone for the development of a completely new concept of biomimetic neuroprosthetic tools activated by light with a straightforward and novel applications in the field of functional restoration in retinal dystrophies and, more generally, in neurodegenerarative diseases.

Introduction

Early synaptic dysfunctions are responsible for a large number of neurological disorders, including epilepsy, autism, Parkinson's disease, and traumatic brain injuries, many of which are drug-resistant. In these cases, neural stimulation with microelectrodes represents the gold-standard therapeutic benchmark at the clinical level. Nevertheless, the scientific community has focused on novel techniques that outperform electrical stimulation regarding resolution and invasiveness, moving towards a more biomimetic recovery of the functions lost by the diseased brain tissue.

Chemical stimulation by local delivery of inhibitory or excitatory neurotransmitters represents a biomimetic strategy capable of recovering chemical synaptic activity that is altered by the disease.[1–3] Dopaminergic or glutamatergic stimulation, for instance, has long been reported to elicit modulation of neuronal activity *in vitro* and *ex vivo*, highlighting its potential for brain therapeutics.[4–6] In the last decades, advancements in drug delivery systems, such as surface-functionalized nanoparticles loaded with specific cargos, have increasingly enabled

[a] *Plasmon Nanotechnology, Istituto Italiano di Tecnologia, Genova, Italy. E-mail: francesco.deangelis@iit.it*
[b] *CINBIO Universidade de Vigo, Vigo, Spain*
[c] *Center for Synaptic Neuroscience and Technology, Istituto Italiano di Tecnologia, Genova, Italy. E-mail: elisabetta.colombo@iit.it*
[d] *The Open University Affiliated Research Centre at Istituto Italiano di Tecnologia (ARC@IIT), Genova, Italy*
[e] *IRCCS Ospedale Policlinico San Martino, Genova, Italy*
[f] *Department of Neuroscience (DINOGMI), University of Genoa, Genova, Italy*
[g] *Bio-Organic Chemistry, Department of Biomedical Engineering, Institute for Complex Molecular Systems (ICMS), Eindhoven University of Technology, Eindhoven, The Netherlands*

† Electronic supplementary information (ESI) available. See DOI: https://doi.org/10.1039/d5mh00082c

‡ Equal contribution.

the targeting of the central nervous system (CNS) with effective localized doses.[7–9] These particles can release their cargo upon a specific stimulus such as pH, temperature, magnetic or electric fields.[10,11] While injectable nanocarriers have undeniable potential for drug delivery to the CNS, the blood–brain barrier (BBB), the natural barrier that protects the brain from pathogens and toxins,[12] renders systemic administration of neuroactive drugs very challenging. Brain-implanted devices equipped with reservoirs with a storage-and-release function could achieve local and regulated delivery of molecules and drugs that bypass the BBB.[13–16] These reservoir systems rely solely on the diffusion of the drug without the possibility of controlling or triggering its dynamics, and consequently, they are destined to be restricted to chronic pharmaceutical therapies.

Optogenetic tools gained increasing interest as an alternative neural stimulation technique endowed with high target specificity and spatial resolution. By genetically modifying neurons to express light-sensitive actuators, such as microbial opsins or receptor-opsin chimeras, it is possible to excite, inhibit, or metabolically modulate neuronal activity with unprecedented precision and specificity.[17–19] Notwithstanding its potential, genetic manipulation is hampered by a difficult translation to clinical practice due to gene therapy and uncertainties related to long-term effects.

From the birth of optogenetics, light became a very advantageous means to elicit neuronal stimulation thanks to its spatial and temporal resolution and low invasiveness.[20] In the field of light-triggered chemical neurostimulation, a variety of strategies to cage/uncage glutamate, the main excitatory neurotransmitter of the CNS, or activate postsynaptic glutamate receptors have been proposed.[21–23] Among photoswitchable moieties, azobenzene, and spiropyran peak for their big molecular conformational change and polarity switch when subjected to near-ultraviolet (UV)/cyan light, which has been demonstrated to be a paramount feature for stimulus-responsive drug delivery approaches.[24–26]

Here, we propose a planar photosensitive nanodevice that successfully modulates neuronal activity *in vitro* and *ex vivo* by locally releasing glutamate upon near-UV light pulses and acting as a drug barrier upon white light illumination (Fig. 1). Glutamate is released through an array of solid-state nanopores, whose architecture, in terms of pore number and dimension, allows the control of the spatial-temporal dynamics of release.[27] Nanopores are separated from the glutamate reservoir by a thin spiropyran film that acts as a photo-barrier, switching between open and closed conformations and allowing for the controlled efflux of glutamate towards neuronal cells or tissues upon illumination. The polymer dynamics showed a complete opening of the nanovalve over a few seconds with a release rate of about 60 μM h^{-1}. We show that the nanovalve is cytocompatible and capable of driving firing activity in primary neurons grown onto the device and blind retinal explants. The data demonstrate the ability of the photosensitive device to mimic activity-dependent glutamate release and reconstitute hybrid synaptic connections with potential applications in the field of neurodegeneration and vision restoration.

Results

Characterization of the pSMA polymer thin film

Spiropyran photoactive moieties were synthesized in a methacrylate-based backbone *via* free radical polymerization. The spiropyran moiety was chosen due to its ability to reversibly change its polarity upon irradiation resulting in an increased dipole moment μ from 4.3 D to 17.7 D,[28] thereby recapitulating the mechanism of a valve, *i.e.*, "closed" when hydrophobic and "open" when hydrophilic. These functional groups require near-UV light to switch to merocyanine conformation and reverse back by visible light (Fig. 2(a)). The structure and purity of the poly(spiropyran methacrylate) polymer (pSMA) were confirmed by proton nuclear magnetic resonance spectroscopy (^{1}H-NMR), while gel permeation chromatography (GPC) was employed to measure pSMA molecular weight and dispersion, resulting in M_w = 13 570 g mol^{-1}, M_n = 7370 g mol^{-1}, and

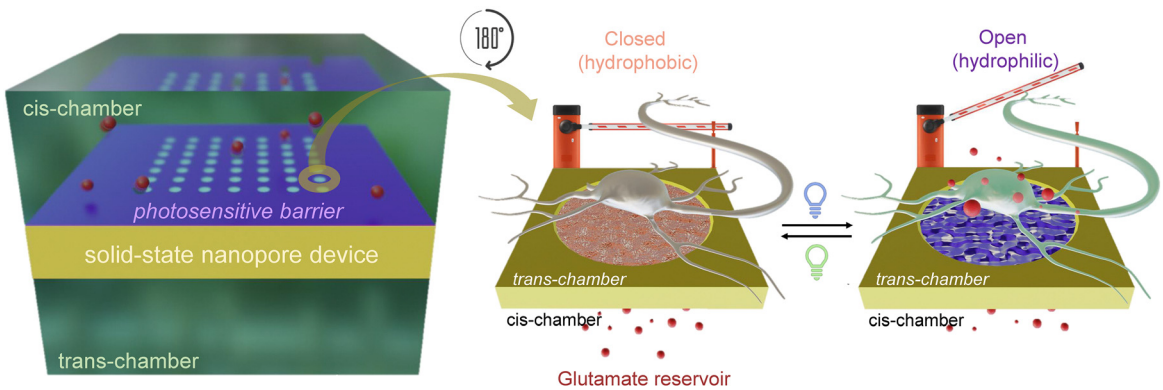

Fig. 1 Scheme of the photosensitive nanovalve. A solid-state nanopore-array device, functionalized with the photosensitive spiropyran polymer, is placed between two chambers (*cis*- and *trans*-), acting as a photo-switchable barrier (left). The neurotransmitter glutamate is loaded in the *cis*-chamber (reservoir) and is released by diffusion to the *trans*-chamber. When the barrier is closed (hydrophobic conformation), glutamate cannot pass through the nanopores (middle). After the light stimulus, the barrier opens (hydrophilic state) allowing the translocation of the molecule and the stimulation of the neurons layered on the device (right).

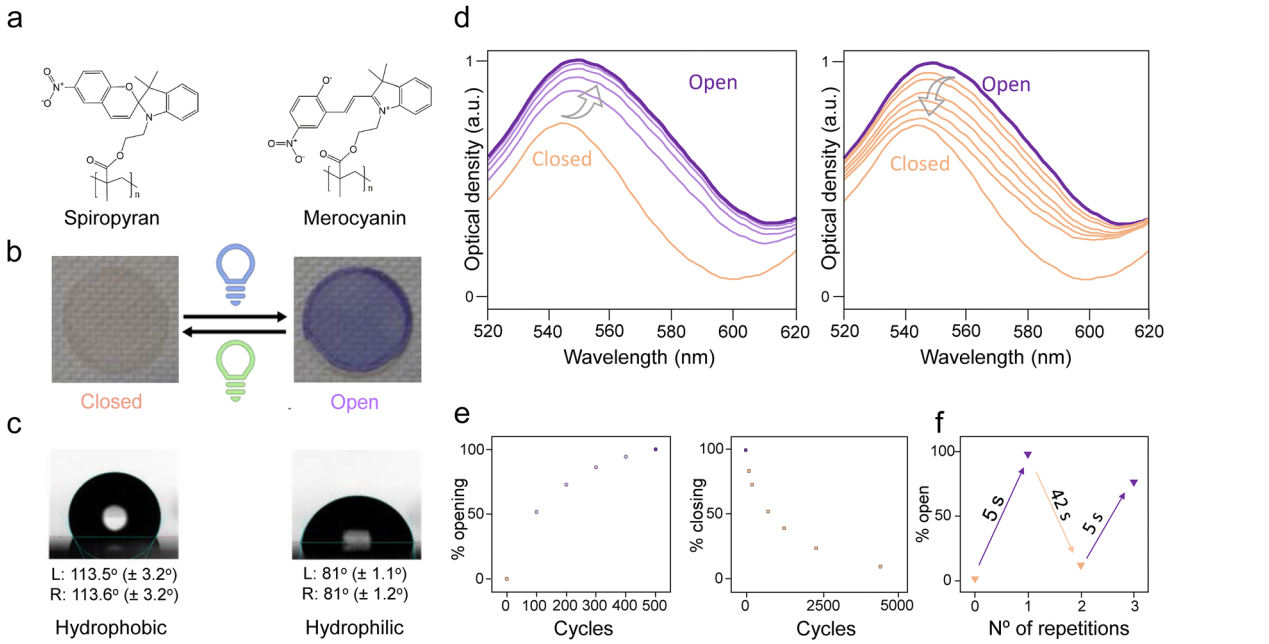

Fig. 2 Conformational change of the spiropyran-based polymer upon illumination. (a) Spiropyran moiety (neutrally charged) changes to merocyanine (ionically charged) after UV exposure due to the heterocyclic break of the C–O bond. (b) The spin-coated polymer onto a glass coverslip (10 mg mL^{-1} in THF, 50 μL, 800 rpm, 60 s) changes color from pink (closed conformation) to purple (open conformation). (c) Contact angle measurements of a drop of water onto the functionalized coverslip show a hydrophobic surface on the closed conformation (>90°) and a hydrophilic surface in open conformation (<90°). (d) Absorbance spectra monitoring the transition from closed to open conformation (left) and *vice versa* (right). (e) Representation of the percentage of aperture (left) and closure (right) *versus* the number of irradiation cycles, both showing an exponential behaviour. (f) Reversibility of the switching between the closed and open conformations.

$Đ$ = 1.84 (Fig. S1a and b, ESI†). To demonstrate the polymer photoswitching ability, pSMA dissolved in tetrahydrofuran (THF; 50 μL of 10 mg mL^{-1}) was spin-coated onto a glass coverslip. The pSMA polarity switch was observable thanks to a color change from pink (closed conformation) to purple (open conformation) upon UV exposure (Fig. 2(b) and Fig. S1c, ESI†). Contact angle measurements of the pSMA film were performed under 565 and 405 nm irradiation, showing a transition from a hydrophobic (113°) to a hydrophilic state (81°), as shown in Fig. 2(c), while the control glass coverslip without polymer showed a contact angle of 43°. The altered hydrophobicity of the film confirms the charge change from neutral to zwitterionic, exploitable to control delivery and retention of water-dispersed molecules, such as the here proposed glutamate.

We then assessed the switching dynamics of the pSMA film from open to closed configuration by means of optical spectroscopy (Fig. S2, ESI†). The illumination protocol was chosen to avoid thermal toxicity in the following experiments with cells and tissues. We employed a blue-shifted wavelength (400 nm) to elicit a hydrophilic change in the structure of pSMA instead of the peak UV absorbance of the polymer (~365 nm) to mitigate potential cell damage, while a combination of 500, 540, and 580 nm was used to revert the process. We applied repeated 20-ms pulse stimulations (50% duty cycle) to establish a correlation between exposure time and conformational changes while measuring the absorbance of the pSMA in the 520–620 nm wavelength range following light excitation (Fig. 2(d)). The peak absorbance in the hydrophobic conformation at 548 nm showed an increase upon 100 cycles, reaching a red shift of about 7 nm after 500 cycles. The pSMA absorbance remained stable with further illumination, demonstrating a complete conversion of the polymer conformation after 500 cycles. When the white light combination (500, 540, and 580 nm) was employed to reverse the conformation back to hydrophobic (closed), an absorbance to 10% of the value measured in the hydrophilic (open) configuration was achieved with over 4000 cycles. This indicates that reforming the C–O bond in the spiropyran moiety requires more energy and, consequently, more time than their dissociation.[24] Both illumination protocols fit an exponential curve describing the conformational change to "open" and "closed" configurations (Fig. 2(e)) that is reproducible in time, as expected for a neurostimulation tool (Fig. 2(f)).

The photosensitive polymer does not affect neuronal viability and activity

We then asked whether the photosensitive polymer was cytocompatible when in contact with neural cells *in vitro*. For this purpose, we plated primary neurons on either pSMA thin films or bare glass coverslips used as controls. Neurons layered on the polymer were kept in the dark in the incubator for 12 days *in vitro* (DIVs) and then characterized for their morphology, viability, and electrophysiological properties. Neurons showed similar neurite outgrowth both on polymer-coated and control substrates, as demonstrated in Fig. 3(a) by β-tubulin immunoreactivity labeling of dendrites and axons. The viability of neurons in contact with pSMA was comparable to that of

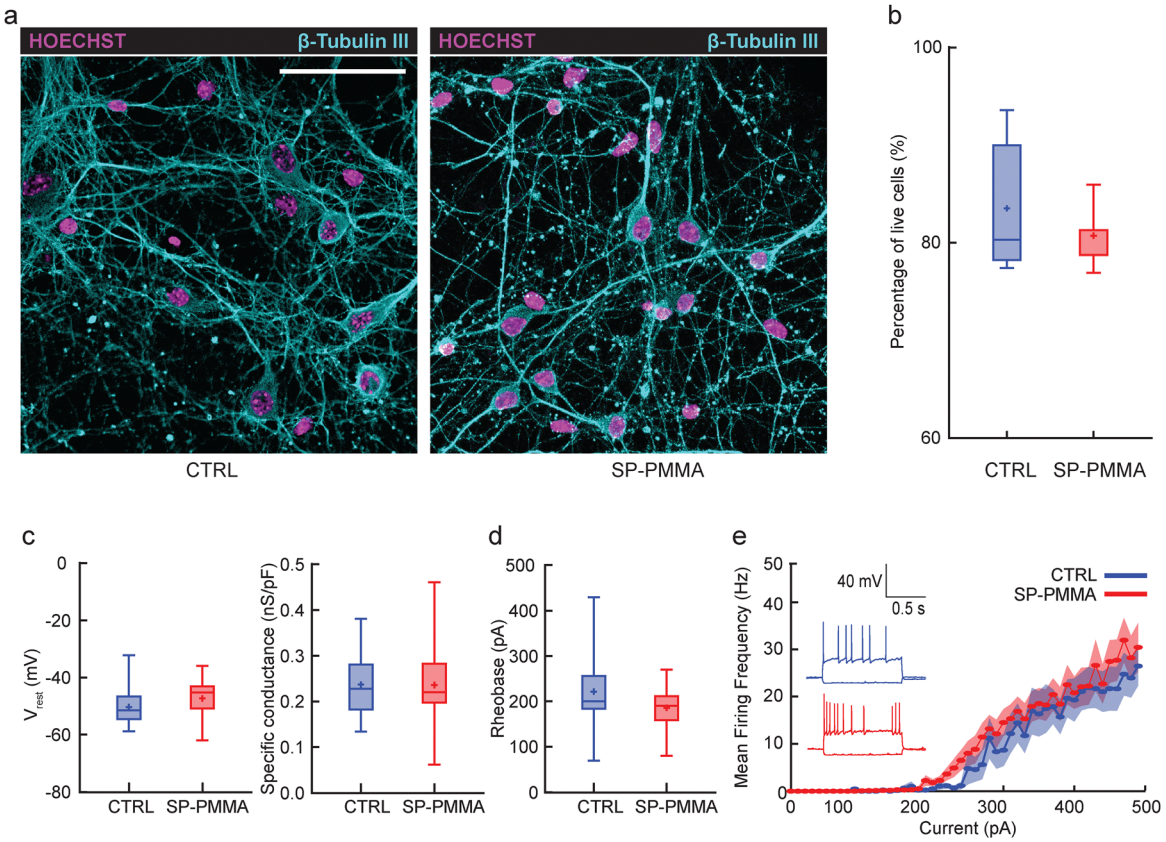

Fig. 3 Cytocompatibility of pSMA in contact with primary neurons. (a) Representative confocal images of primary neurons plated either on glass coverslips (left, CTRL) or on glass coverslips spin-coated with pSMA (right). Scale bar, 50 μm. Neurons were stained with Hoechst and β-Tubulin III to visualize nuclei and neurite morphology respectively. (b) Neurons were live stained with Hoechst for total cell counts and Propidium Iodide (PI) for dead cells. Cell viability was quantified as the ratio between live cells and the total number of cells. Cell viability remains unchanged regardless of the plating substrate (CTRL *vs.* pSMA). (c) Passive electrophysiological parameters obtained by whole-cell patch clamp show no influence of the plating substrate on the resting potential (left panel) and specific conductance (right panel). (d) Rheobase values obtained with current-clamp step protocols are not altered in both experimental groups (CTRL *vs.* pSMA). (e) Firing activity evoked by injecting increasing steps of current (inset) show no differences between neurons plated on either CTRL or pSMA-coated coverslips (right panel). Viability: n = 9 for both CTRL and pSMA cultured coverslips; Student's t-test. V_{rest}: n = 15 and 17 for CTRL and pSMA, respectively; Mann–Whitney U-test. Specific conductance: n = 15 and17 for CTRL and pSMA, respectively; Student's t-test. Rheobase: n = 15 and 16 for CTRL and pSMA, respectively; Student's t-test. Mean firing frequency: n = 15 and 16 for CTRL and pSMA, respectively; Student's t-test. Primary neurons were obtained from at least n = 3 independent preparations.

neurons grown under control conditions (Fig. 3(b)). Moreover, their passive electrophysiological properties, such as resting potential, specific conductance, and current density, were not affected by the contact with pSMA (Fig. 3(c)). The firing activity and response to depolarizing currents (rheobase, *i.e.* the current needed to reach the firing threshold) showed physiological values in both experimental groups (Fig. 3(d) and (e)). Taken together, the data demonstrate an excellent cytocompatibility of the photosensitive surfaces in contact with primary neurons up to 12 DIVs.

Design of the photosensitive nanovalve

The nanovalve system consists of a solid-state nanopore array on a suspended membrane located between two chambers and covered with pSMA. The *cis*-chamber (back side) serves as a reservoir, while the *trans*-chamber (top side) is where glutamate is translocated, and cells and tissues are interfaced. We engineered a chip of 14 × 14 mm in size composed of a 2 × 2 mm Si_3N_4 membrane of 500 nm thickness (Fig. 4(a)) out of a scaffolding 500-μm silicon (Si) wafer sandwiched between two layers of silicon nitride (Si_3N_4). For the fabrication of the nanovalve, a metal mask was used to print the 2 × 2 mm window on the back side of the Si wafer, previously covered with S1813 photoresist and then exposed to UV light. Trifluoromethane (CHF_3) reactive ion etching (RIE) was then employed to remove the Si_3N_4 from the designed 2 × 2 mm window. Si was then wet-etched in potassium hydroxide (KOH), leaving the residual Si_3N_4 layer exposed on both the top and back side of the chip within the 2 × 2 mm window. A 5-nm titanium (Ti) and a 20-nm gold (Au) layers were evaporated onto the top side of the Si_3N_4 suspended membrane to furnish electrical conductivity and avoid the accumulation of charge when exposed to the electron or ion beam during focus ion beam (FIB) procedure (Fig. S3a–h, ESI†). Accordingly, the membrane was milled with the selected pattern using FIB and characterized by scanning electron microscopy (SEM). Each hole has a diameter of

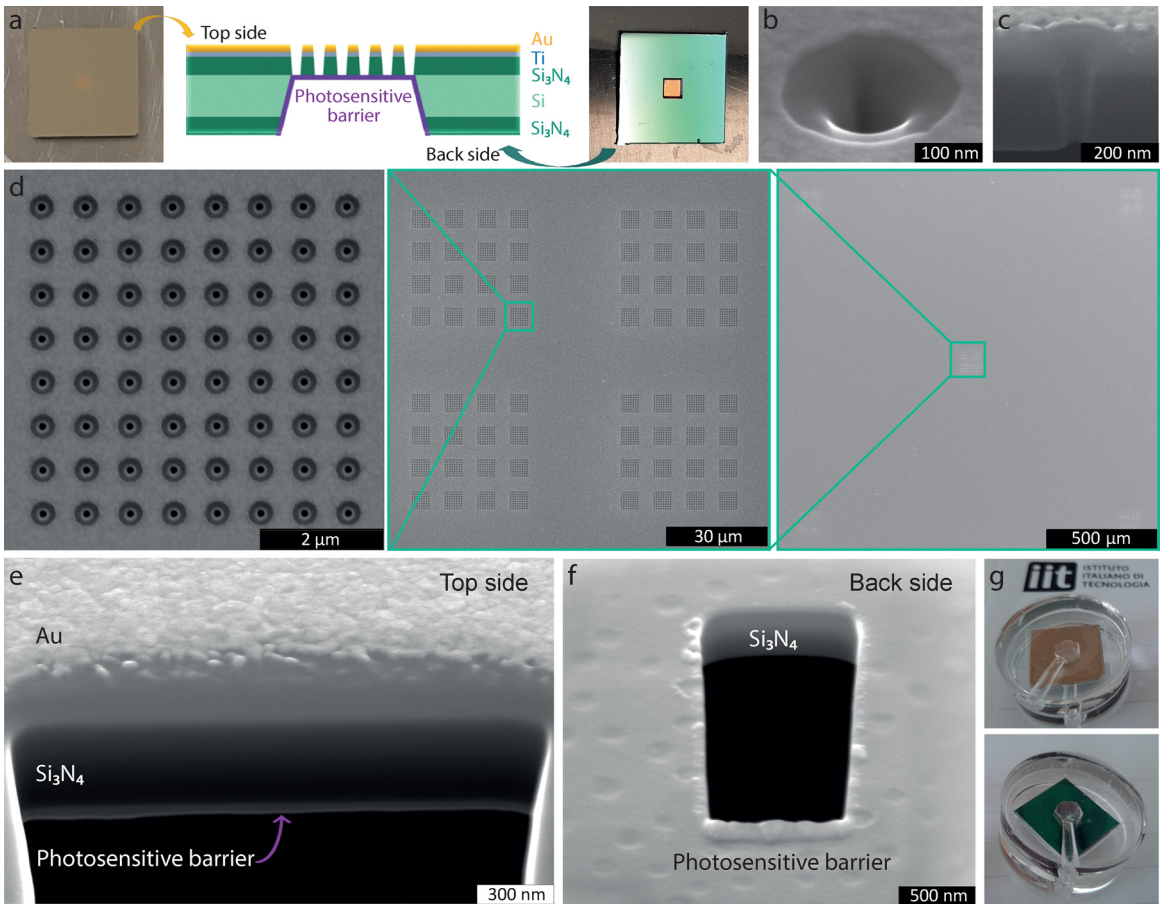

Fig. 4 Design and morphological characterization of the photosensitive nanovalve. (a) Top and back view of the chip: the window (2 × 2 mm) is placed in the center of the chip, surrounded by the frame (14 × 14 mm). The cross-section is outlined showing the distinct layers that compose the device. From top to bottom, the frame is composed of Au (20 nm), Ti (5 nm), S_3N_4 (500 nm), Si (500 μm), and S_3N_4 (500 nm). The window is composed of Au (20 nm), Ti (5 nm), S_3N_4 (500 nm), and pSMA (70 ± 10 nm). (b) SEM image at 52° of a single-pore (100 nm diameter); (c) and its cross-section showing the V-shaped hole through the window. (d) Design of the nanopore array pattern, named checkboard (left) Nanopore array patterns arranged in a bigger square, 8 × 8, each one separated by 700 nm (middle). Final distribution of the bigger squares on the corners and middle portion of the device (right). (e) Cross-section of the device seen from the top of the window: pSMA (deposited on the back) is represented in light grey. (f) Cross-section from the back of the S_3N_4 membrane covered with pSMA showing the homogeneous deposition. (g) The nanovalve is composed of the device inserted into the PDMS holder engineered for the glutamate translocation measurements, seen from the top (up) and the back (down).

100 nm (Fig. 4(b)) and shows the usual V-shape in the cross-section (Fig. 4(c)). Nanostructures are arranged in a 5 × 5 μm square with a pitch of 700 nm (Fig. 4(d), left), composing four 4 × 4 arrays made of 64 pores each (Fig. 4(d), middle). This pattern is milled at the corners and center of a 1.5 × 1.5 mm suspended window (Fig. 4(d), right) containing a total of 20,480 nanopores. Considering the timing of glutamate diffusion in a standard culture medium, this checkboard design ensures five quasi-independent neurotransmitter release locations for cells and tissues layered on the chip surface, thereby allowing the characterization of spatially distinct areas within the same biological preparation.

Finally, the chip is functionalized on the back side with the pSMA polymer, which acts as a photosensitive barrier. To this aim, 10 μL of 1 mg mL^{-1} pSMA solution in THF is drop-casted at 70 °C on the chip, achieving a homogeneous layer of polymer of 70 ± 10 nm thickness (Fig. 4(e) and (f)). To create the final nanovalve device, a polydimethylsiloxane (PDMS) holder with a *cis*- and a *trans*-chamber on the top and back sides of the device was designed (Fig. 3(g)). Each chamber has a capacity of 100 μL and is equipped with inlet and outlet for filling and washout.

The delivery of glutamate through the photosensitive array of the nanovalve is regulated by light

To assess the diffusion of glutamate, its concentration was measured over time by withdrawing aliquots from the *trans*-chamber, with the *cis*-chamber serving as a reservoir. To compare the free diffusion of the molecule through the solid-state nanopores with respect to the diffusion hindered when the pSMA is fully closed, two scenarios were examined: (i) a device lacking pSMA allowing unrestricted diffusion of the molecule; and (ii) a device functionalized with the polymer acting as a photosensitive hydrophobic barrier. The initial concentration of glutamate in the *cis*-chamber was 45 mM in both cases, and aliquots were collected every hour from the *trans*-chamber. A glutamate assay kit was employed to assess the concentration by measuring fluorescence with a plate reader (λ_{ex} = 540 nm, λ_{em} = 590 nm). Both in the

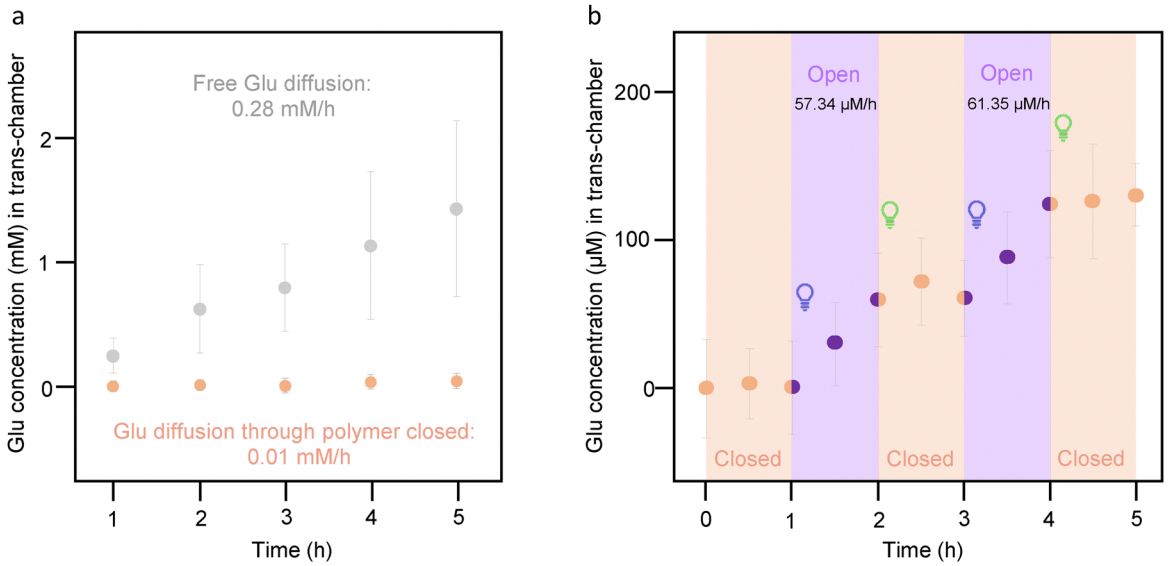

Fig. 5 Glutamate delivery by the nanovalve is activated "on-demand" by illumination. (a) Comparison between the free diffusion of glutamate through a solid-state nanopore device without pSMA (grey symbols), and efflux of glutamate through the pSMA-coated nanopores with the polymer in the closed conformation (orange symbols) Error bars correspond to standard error. The release is hindered up to 96% after 5 h. (b) Evaluation of the nanovalve switching between the closed and open pSMA conformation. The rate of delivery is significantly increased when SP-PMMA is in the hydrophilic conformation. Data are presented as mean ± standard error of n = 3 samples.

absence of pSMA (free glutamate diffusion) and in the presence of the "closed" hydrophobic polymer (Fig. 5(a)), the glutamate translocation followed a linear regression and confirmed that glutamate release was hindered by 96% after 5 hours of the experiment. In the presence of the polymer, the rate of glutamate diffusion was 10 μM h^{-1}, while the free diffusion through the solid-state nanopores reached a rate of 280 μM h^{-1}.

The next step was to check the potential of pSMA as a switching-on and switching-off barrier, regulating the rate of glutamate delivery. To this purpose, the nanovalve was fabricated with a device functionalized with pSMA as described above and filled with 45 mM of glutamate in the *cis*-chamber, as in the previous experiments. Three aliquots were withdrawn every 30 min and analyzed with the glutamate fluorometric assay. Subsequently, irradiation with 400 nm light for 500 cycles at the same frequency reported for the characterization of the pSMA film was applied, and two more aliquots were collected every 30 min. Finally, 4200 cycles were applied with a combination of 500 nm, 540 nm, and 580 nm, similarly to the experiments on the film, and two more aliquots were analyzed. The process was repeated twice. Fig. 5(b) shows that the diffusion rate is considerably lower when the pSMA is closed than when it is open, showing a release rate of approximately 60 μM h^{-1} upon illumination at 400 nm, while glutamate outflow can be stopped upon irradiation with visible light. This result proves the potential use of this device as a wireless nanovalve for the controlled release of glutamate that can potentially be extended to other kinds of polar molecules or bio-probes.

Light-driven glutamate diffusion through the nanovalve stimulates primary neurons

We then asked whether the nanovalve device could be exploited for the stimulation of neurons at different levels of network complexity. For this purpose, we first cultured primary hippocampal neurons on the nanovalve chip for 12 DIVs following the same procedure used for the cytocompatibility experiments and then performed patch-clamp recordings to assess the neuronal response to glutamate diffusion through the nanopores upon illumination. The illumination followed a similar pattern with respect to the one investigated for the characterization of the switching dynamics of the pSMA (10 ms stimuli, 50 Hz). We intercalated periods of dark and pulsed near-UV or green light illumination cycles while recording neuronal activity in cell-attached patch-clamp configuration (Fig. 6(a)). We selected the neurons sitting in the proximity of the pores and restricted the illumination mostly to the cell soma as depicted in Fig. 6(b). We loaded either glutamate or extracellular solution (Tyrode) beneath the device and performed repeated light stimulation in the near-UV range (Fig. 6(c), purple boxes purple bars, sequence of trains of 30 pulses at 50 Hz, duty cycle: 50% and 600 ms of darkness, 10 + 10 + 20 sequences). While loading glutamate in the *trans* chamber induced a significant light-dependent increase in neuronal firing, control cells (Tyrode) were not affected by light stimulation (Fig. 6(d)), ruling out the involvement of thermal effects. As shown by the peristimulus time histograms (PSTHs) of two representative recordings (Fig. 6(e) and (f), left), the latency of light-evoked responses was consistent with the dynamics of the pSMA conformational change studied by optical spectroscopy and the time needed for glutamate diffusion to reach a physiologically active concentration. When the process was reversed by illuminating the device with white light (green bars) cycles, the firing activity decreased progressively to basal levels, as expected upon a diminished excitatory neurotransmitter delivery. The right insets of Fig. 6(e) and (f) show in more detail the basal activity traces of the neurons (light blue), their increased action potential firing

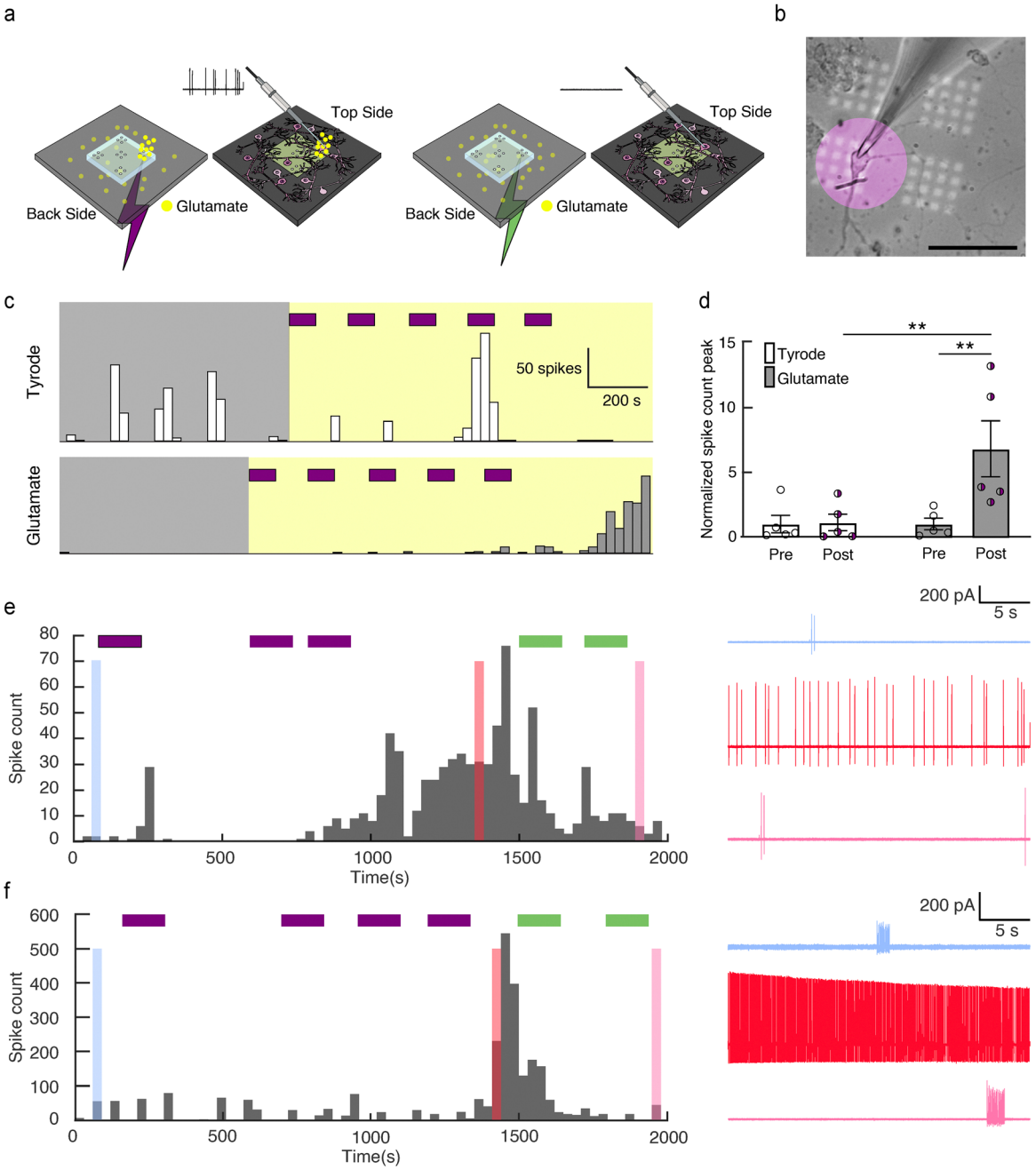

Fig. 6 Glutamate-driven stimulation of primary neurons by the photosensitive nanovalve. (a) Schematic representation of the experimental setup. The polymer was drop-casted on the back side of the nanodevice in correspondence of the nanopore array. Then, glutamate (10 mM, yellow dots) was loaded on the back side, and primary neurons were plated on the top side of the nanodevice. Neuronal activity was recorded by patch-clamp from the top side. (b) Representative image of a recorded neuron seating on the nanopore array with the superimposition of the light stimulation spot (50 μm in diameter). Scale bar, 50 μm. (c) Representative spike count histograms (30-s bin) from one cell stimulated by light-triggered glutamate release and one control cell exposed to the same optical stimulation but perfused with extracellular solution (Tyrode) instead of glutamate. Light stimulation (violet boxes) consisted of a sequence of near-UV stimulation protocols, each composed of a sequence of 10, 10, and 20 repetitions of a train of 30 light pulses (50 Hz, 50% duty cycle), interspersed by 600 ms of dark. Grey and yellow shaded boxes depict pre- and post-stimulation time windows. (d) Quantification of the light-induced effect on neuronal firing: the maximum spike count was measured before and after optical stimulation (pre *vs.* post). Control cells (Tyrode) showed no increase in firing, whereas glutamate-stimulated cells exhibited a significant increase upon light-induced glutamate release. (*$p < 0.05$, **$p < 0.01$, two-way ANOVA with uncorrected Fisher's LSD test, $n = 5$ cells and 5 devices for both Tyrode and Glutamate conditions). (e), (f) Representative peri-stimulus time histograms (PSTHs) of spike counts (left panels, 30-s bins) of 2 cells subjected to light-triggered glutamate stimulation (violet and green boxes) by the nanodevice and representative 30-s traces (right panels) prior to illumination (cyan bar) after near-UV light stimulation (red bar) and after white-light stimulation (pink bar). Traces refer to the time windows labeled with color-matched bars in the time histograms. Focused white light stimulation (green arrow in a: 475 nm, 44 mW mm^{-2} + 510 nm, 10 mW mm^{-2} + 555 nm, 54 mW mm^{-2}) causes polymer closure, inhibiting glutamate efflux. This results in the lack of neuronal activation on the top side of the device. On the contrary, near-UV light stimulation (violet arrow in a; 390 nm, 100 mW mm^{-2}) triggers polymer opening and nanopore-mediated glutamate diffusion, which in turn stimulates neuronal firing. Both neurons display near-UV light-triggered firing and firing inhibition mediated by white light, albeit with various timings and magnitudes.

upon near-UV opening of the polymeric barrier (red), and the final recovery to basal firing upon nanovalve closure (pink).

Light-driven glutamate diffusion through the nanovalve stimulates retinal ganglion cell firing in blind retinas

Once we verified the photostimulation capability of the nanovalve system on a simple model of neuronal network, we sought to demonstrate its potential as a neurostimulation strategy by testing blind retinal explants layered on the device surface. The retina is a well-established model of a complex neuronal network processing visual information. Blind, dystrophic retinas lack photoreceptors and thereby do not respond to light because of the denervation of the inner retinal networks. Thus, they represent an ideal application of the proposed technology as a retina prosthesis restoring the missing light-dependent glutamate release by photoreceptors. To this aim, we dissected the retina of 2-month-old dystrophic Royal College of Surgeons (RCS) rats, an experimental model of *Retinitis pigmentosa*. RCS rats express a mutation in the *Mertk* gene that hinders the phagocytosis of the outer photoreceptor segments by the retinal pigment epithelium (RPE), resulting in the dysfunction and subsequent death of both rods and cones.[29] Retinal explants were layered on the devices, as shown in Fig. 7(a), with the external retina devoid of photoreceptors in contact with the nanovalve and the retinal ganglion cells (RGC) layer exposed to the extracellular medium (AMES medium, USBiological Life Science). Fig. 7(b) shows a representative retina positioning onto the nanovalve array together with the visualization of the various layers of the hybrid retina device. We then performed patch-clamp experiments on RGCs upon removal of the outer limiting membrane by employing a similar protocol to that used for primary neurons for the opening and closing of the photosensitive nanovalve. We recorded the responses from the RGCs overlaying the nanopore source of glutamate and focused the illumination on the same area. The release of glutamate, triggered by near-UV light, induced opposite reactions in the responses of RGCs by inducing either an increase or a decrease in firing rate, as depicted by the PSTHs of two representative cells in Fig. 7(c) and (d). Overall, the release of glutamate by the nanovalve in the outer retina recapitulates the physiological activation of OFF bipolar cells and the concomitant inhibition of ON bipolar cells in the neuroretina, ultimately leading to the activation of OFF-RGC (Fig. 7(c)) and inhibition of ON-RGC firing (Fig. 7(d)).

Discussion

This work presents an innovative and versatile method to deliver molecules in a light-controlled manner through a solid-state nanopore device coated with a photoswitchable pSMA polymer. The findings indicate that when pSMA is in the closed hydrophobic conformation, it effectively inhibits the release of polar molecules, such as glutamate, while when it switches to open, hydrophilic conformation, it allows glutamate to promptly diffuse. Under the latter condition, the developed nanovalve can deliver glutamate at a rate of approximately 60 $\mu M\ h^{-1}$, markedly reducing this rate when the barrier is closed. This validates its function as an on-demand light-driven barrier.

The key point lies in the presence of the spiropyran moiety that, compared to other photosensitive moieties, possesses the advantage of altering the chemical structure, thereby influencing hydrophilicity.[24–26] This characteristic makes it an exceptional candidate for operation in aqueous solvents or buffers commonly used in biological applications. Although the switching times are not within the microscale range, pulses lasting milliseconds, rather than continuous irradiation, can be employed, aligning with the illumination protocols employed for neuronal stimulation. Furthermore, this approach offers the possibility to adjust the delivery rate by partially opening the polymer, thereby saving time, and minimizing unnecessary exposure to irradiation.

Notably, the pSMA-coated nanostructure was demonstrated to be extremely cytocompatible and tissue-friendly, with primary neurons grown in contact with the device for more than 10 days. Neurons preserved their viability and ability to elongate processes and generate a network. Moreover, their passive and active electrophysiological properties, which are sensitive proxies of neuron health, were indistinguishable from neurons grown under standard conditions. These findings open up the possibility of emulating light-driven synaptic transmission by releasing glutamate "on demand".

Synaptic structures are characterized by specialized regions known as active zones, which are 200–500 nm in length[30] and release neurotransmitters from synaptic vesicles containing up to 40 000 molecules.[31] Our device achieved a controlled maximal release rate of approximately 8×10^{-17} mol s^{-1} per nanopore in the hydrophilic configuration, a value that is in the range of synaptic release. In particular, the rate achieved by the photosensitive nanovalve matches the release rate at ribbon synapses of the sensory system, among the few synaptic sites in which the rate of glutamate release is gradually regulated by variations in the membrane potential. In photoreceptors, for instance, the maximal release rate occurs in the darkness, where glutamate is released from multiple sites within individual terminals with up to 400 synaptic vesicles/ribbon, corresponding approximatively to 10^{-17} mol s^{-1}.[32]

When the photoswitchable polymer is illuminated with repeated pulses of "opening" light, it induces an effective photostimulation of action potential firing in primary neurons grown onto the nanopore/polymer device. Moreover, a potential application in reinstating glutamatergic transmission in neural tissue hit by neurodegeneration was demonstrated by its ability to reactivate light responses from light-insensitive retinas in which inner retinal neurons have been denervated by photoreceptor degeneration. Interestingly, glutamate-releasing "opening" light pulses elicited either excitatory or inhibitory responses in distinct RGC populations, consistent with the physiological arrangement of glutamate-dependent ON and OFF pathways processing light and dark information, respectively. In fact, glutamate release in the outer retina activates cone OFF bipolar cells (BCs) bearing AMPA/kainate receptors, while it inhibits rod

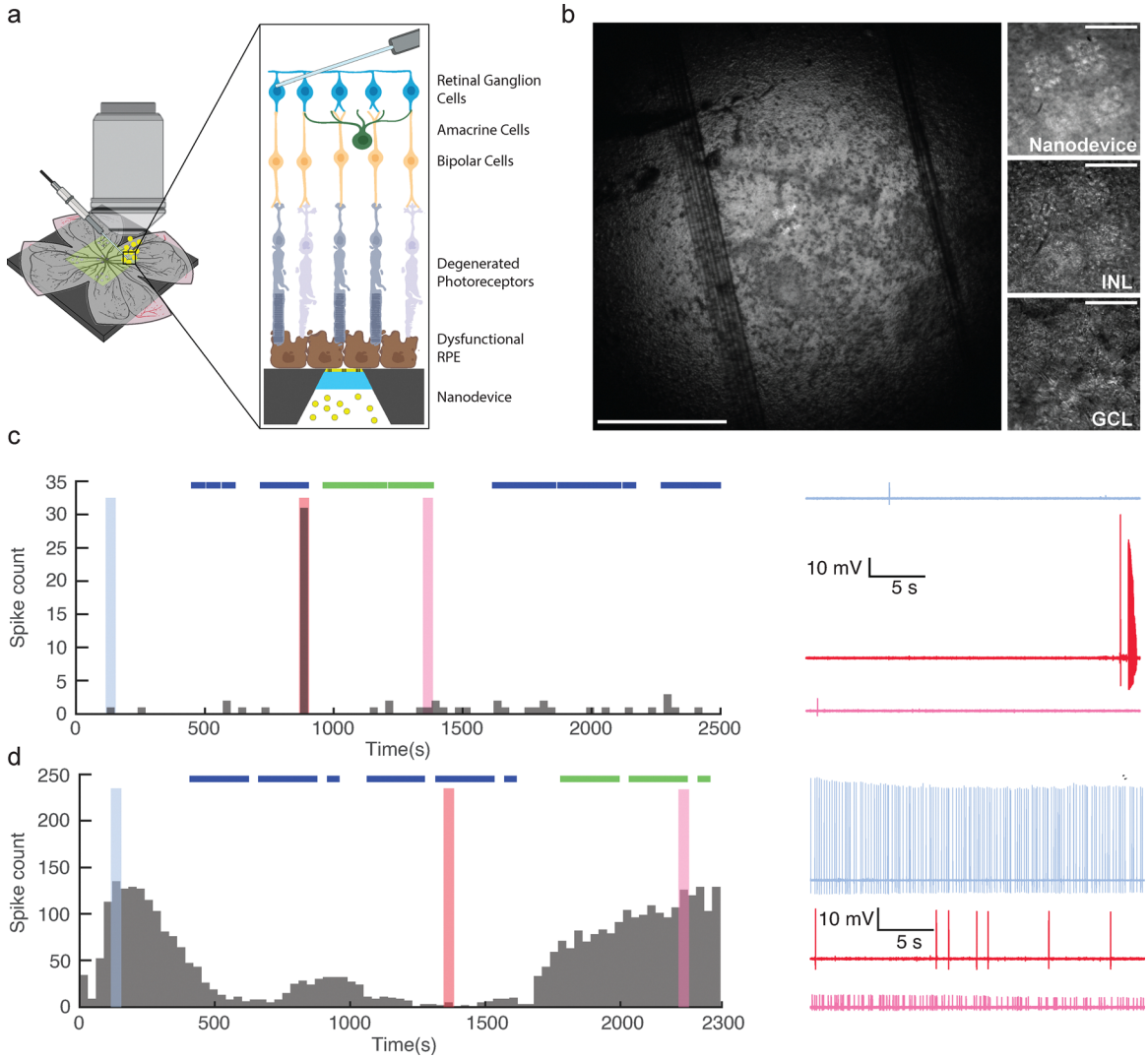

Fig. 7 Light-evoked ON and OFF responses of retinal ganglion cells in blind retinal explants by the photosensitive nanovalve. (a) As shown in Fig. 5, the polymer was drop-cast on the back side of the device and the reservoir was filled with glutamate (yellow dots, 10 mM). Retinal explants from RCS rats affected by photoreceptor degeneration were placed on top of the device with retinal ganglion cells (RGCs) up. Light stimulation was delivered through an upright microscope to trigger either polymer opening (violet light, 390 nm, 85 mW mm^{-2}) or closing (green light, 475 nm, 317 mW mm^{-2}). While light-regulated glutamate release occurred on the side of degenerated photoreceptors, the resulting activity of RGCs was recorded by patch-clamp in the current-clamp configuration. (b) Representative image of a retinal explant placed on top of the nanodevice (left). The magnified schematic on the right displays, from top to bottom, the nanodevice plane, the inner nuclear layer (INL), and the ganglion cell layer (GCL). Scale bar, 50 μm. (c) and (d) Light-mediated modulation of RGC activity. Light stimulation consisted of a sequence of near-UV and green protocols (violet and green boxes). Peristimulus time histograms (PSTHs) of spike counts (left panels, 30-s bins) of 2 RGCs responding to the light-triggered glutamate release in the upstream retinal network and representative 30-s traces (right panels) prior to illumination (cyan), after near-UV light stimulation (red) and after green light stimulation (pink). Traces refer to color-matched bars in the time histograms. The two RGCs display opposite near-UV light-triggered firing responses (c, enhancement; d, suppression), as well as recovery of the firing rate upon green light stimulation, albeit with different timings and magnitudes. The increase and decrease in the firing rate observed in the two RGCs, respectively, are likely due to the opposite effects of glutamate on cone-OFF BCs and on rod and cone-ON BCs and to the activation of the horizontal and amacrine cell network modulating in opposite ways ON- and OFF retinal responses.

and cone ON BCs, bearing hyperpolarizing metabotropic glutamate receptors type 6. In turn, ON-BCs excite ON-RGCs, OFF-BCs excite OFF-RGCs. Additionally, glutamate can activate horizontal cells in the outer plexiform layer, leading to lateral inhibition of BCs, and amacrine cells in the inner plexiform layer, leading to reciprocal effects on RGC activity.[33,34]

The limitation of the relatively long switching times can be potentially overcome by introducing chemical modifications into the molecular structure of the pSMA, potentially improving the conversion process. Additionally, a combination of the photosensitive polymer with plasmonic nanoparticles to enhance the localized surface electric field under irradiation would reduce the switching time. Other potential limitations of the device are the near-UV wavelength necessary to open the polymeric valve and the need for longer wavelength illumination to bring it back to the closed conformation. Given the low tissue penetration and

large scattering of near-UV light, the application of the nanodevice for *in vivo* neural stimulation would benefit from chemical modifications to red-shift the opening wavelength, as well as spontaneous relaxation to the closed state, to require only a single stimulation to have a transient pulse of glutamate onto receptive cells, mimicking the physiological neurotransmitter release dynamics.

The adaptability of this nanovalve enables its use not only for delivering glutamate but also for administering other small molecules, peptides, or even oligonucleotides. Moreover, it can be applied in single-molecule detection by reducing the velocity of molecules passing through the nanopore. The insights gleaned from this study may catalyze the engineering of various valves capable of serving as implants for prolonged and controlled release in medical applications.

Conclusions

In this study, a pSMA-coated nanovalve for on-demand delivery of glutamate through solid-state nanopores has been engineered and assessed for photostimulation of primary neurons and retinal circuits. The current design can be employed for the fabrication of more complex devices for neuronal light-evoked chemical stimulation, as well as for long-term and monitored delivery systems. In conclusion, the results open the possibility of implanting the biomimetic device emulating neurotransmitter release and potentially creating hybrid chemical synapses with neurons to restore neural communication impaired by neurodegeneration.

Methods

Materials and chemicals

Polydimethylsiloxane base elastomer and curing agent (SYLGARD™ 182 Silicone Elastomer) was supplied by Dow Corning. L-Glutamic acid monosodium salt monohydrate and tetrahydrofuran were purchased by Sigma Aldrich. The fluorometric kit for measuring translocated glutamate was provided by Abcam (ab138883). Deionized water was employed in all the experiments.

Synthesis of poly(spiropyran methacrylate) (pSMA)

In a round-bottom flask, equipped with a reflux condenser and a stirring bar, 300 mg (0.851 mmol) of 2-(3′,3′-dimethyl-6-nitrospiro[chromene-2,2′-indolin]-1′-yl)ethyl methacrylate (spiropyran methacrylate), 13.98 mg (0.0851 mmol) of 2,2′-azobis(2-methylpropionitrile) (AIBN), and 2.84 mL of tetrahydrofuran (THF) were added to a final monomer concentration of 0.3 M. A dark purple reaction mixture was obtained and subsequently deoxygenated by bubbling with argon. The polymerization started by lowering the reaction vessel into a preheated oil bath at 60 °C. After 48 h a purple clear mixture was obtained, which was precipitated from ice-cold methanol and dried under vacuum. Hereafter the polymer was dissolved in dioxane and freeze-dried overnight (215.8 mg, ∼72% yield). Structure and purity were confirmed by nuclear magnetic resonance spectroscopy (NMR). Molecular weight was calculated from gel permeation chromatography (GPC), resulting in M_w = 13 570 g mol^{-1}, M_n = 7370 g mol^{-1}, and $Đ$ = 1.84. ^{1}H-NMR spectra were conducted on a Bruker Advance 400 MHz spectrometer ($CDCl_3$). GPC was recorded using a Shimadzu Prominence-i system configured with a PLgel mixed D column, a photodiode array (PDA) detector (254 nm), and a differential refractive index detector. The eluent was THF with a flow rate of 1 mL min^{-1}, and we employed polystyrene calibration standards (Scheme 1).

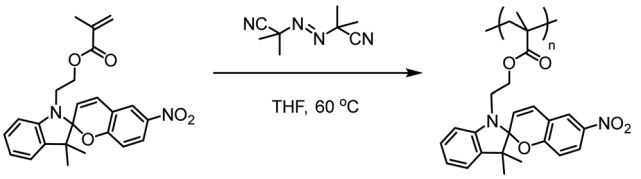

Scheme 1 Synthesis of pSMA *via* free radical polymerization, using azoinitiator AIBN, in THF solvent under reflux.

Optical spectroscopy (Fig. S2, ESI†)

A multi-LEDs source (CoolLed PE800) is connected to a Witec microscope in Kohler illumination mode and is driven by a function generator. With this solution, we were able to achieve an illumination pattern of 50-Hz pulses trains (pulses of 10 ms on and 10 ms off) with selectable length. Using an Olympus 10× LWD objective, we exploited the field aperture to restrict the illuminated area to 150 μm^2. Stimulation: we used only the 400 nm-peaked LED which generated an irradiance of 10 mW mm^{-2}. To achieve the inverse configuration of the polymer, the combination of the LEDs with peak emission at 500 nm, 540 nm and 580 nm was turned on with the same illumination pattern as before (20 ms 50-Hz pulses, 10 mW mm^{-2}). Recording of spectra: to monitor the change of polymer conformation, absorbance spectra were collected with the same microscopy setup. For this purpose, we installed white light illumination (DH 2000 Bal source from Ocean Optics) from below and collected the signal from above through an optical fiber (multi-mode type with 100 μm core) up to an UHTS 300 spectrometer (equipped with 1200 g mm^{-1} grating and Andor Newton Duo 970P EMCCD camera).

Fabrication of the nanovalve (Fig. S3a–h, ESI†)

Photolithography. A 500 μm thick wafer of Si sandwiched between two layers of 500 nm thick layer of Si_3N_4, is covered on the top side with S1813 photoresist through spin-coating (4000 rpm for 60 seconds) and annealed onto a hot plate at 95 °C for 3 min.

Pattern for fabrication of devices with frame 14 × 14 mm and window 2 × 2 mm is printed onto the top side of the wafer under UV exposure (9 s, 350–450 nm broadband exposure) using Süss MicroTec MA6/BA6 mask aligner. The wafer is developed by rinsing 90 s in MF319 developer, and 90 s in deionized water.

Reactive ion etching (RIE). The selected Si_3N_4 layer onto side A is dry-etched by the developed S1813 resist leaving exposed the under-Si layer. SENTECH SI500 RIE instrument is employed with these settings: O_2 flow rate: 5 atm cm^3 min^{-1}, CHF_3 flow rate: 70 atm cm^3 min^{-1}, Time: 1000 s. The wafer is cleaned with acetone to remove residual S1813 resist.

KOH etching. The Si layer is wet etched by dipping the wafer in KOH solution (30 wt%) for 10 hours at 90 °C and rinsed with deionized water. As a result, a 500 nm thick Si_3N_4 window of 2 × 2 mm is opened onto the wafer.

Ti/Au deposition. A 5-nm Ti layer and 20-nm Au layer are deposited onto the top membrane using the Kenosistec KE500ET conjugated e-beam/thermal evaporator.

Milling patterning. Nanopore array is milled onto the Si_3N_4 window and characterized using FEI Helios NanoLab Dual-Beam 650 system, a workstation combining Ga FIB operating a 30 kV (Tomahawk™) and SEM consisting of 30 kV monochromated Schottky FESEM column (Elstar™).

Assembly of pSMA polymer onto the Si_3N_4 membrane devices. 1 mL of 1 mg mL^{-1} spiropyran is dissolved in THF and sonicated in a water bath for 30 min. During this time, the solid-state nanodevice is placed on a hot plate at 70 °C facing up the back side. Ten μL of the previous solution is drop cast onto the Si_3N_4 window and let dry for 5 min. Samples are left to cool down to room temperature (RT).

Development of holder for the nanovalve. PDMS base elastomer and curing agent are mixed in a 10 : 1 ratio and left in the desiccator for 30 min to remove bubbles. A hand-made template was fabricated and filled up with the previous composite and cured at 65 °C for 6 h. After retrieving the template and plasma cleaning, the holder is ready to use.

Immunocytochemistry

Mouse hippocampal neurons were fixed in phosphate-buffered saline (PBS)/4% paraformaldehyde for 15 min at RT and washed three times with PBS. Samples were then incubated overnight with an anti-β-tubulin III primary antibody (mouse monoclonal #801202, BioLegend) diluted in 5% normal goat serum (NGS)/0.1% Triton/PBS. After 4 washes in 20 mM Na_2HPO_4/NaH_2PO_4 with 0.5 M NaCl, samples were incubated for 2 h at RT with fluorescently conjugated secondary antibody (Alexa-488 anti-mouse #A11029, Thermo-Fisher Scientific) diluted in 5% NGS/0.1% Triton/PBS. After 3 washes in 20 mM Na_2HPO_4/NaH_2PO_4 with 0.5 M NaCl and one wash in PBS, samples were incubated for 10 min at RT with Hoechst 33342 and then mounted in Vectashield antifade mounting medium (#H-1000-10, Vector Laboratories) on rectangular coverslips. Image acquisitions were performed using a confocal microscope (SP8, Leica Microsystems GmbH, Wetzlar, Germany) at 40× (1.4 NA) magnification.

Cell viability assay

To assess if pSMA itself was harmful to primary neurons, primary hippocampal neurons at 12 DIVs were stained with propidium iodide (PI, 1 μM) and Hoechst 33342 (1 μM) for 3 min. Impermeable to live cells, PI was used to detect cell death, while Hoechst 33342 was used to stain nuclei for total cell counts. Neuronal viability was quantified by calculating the ratio of PI-positive cells to Hoechst-positive cells. Glass coverslips were used as control to compare pSMA-coated coverslips.

Patch-clamp electrophysiology

To assess pSMA effect on neurons function, whole-cell patch-clamp recordings were made from hippocampal neurons plated on pSMA-coated coverslip or glass coverslip as control. Measurements were conducted on neurons between 11 and 14 DIVs. Patch pipettes, prepared from thin-borosilicate glass (Kimble, Kimax, Mexico) were pulled and fire-polished to a final resistance of 2–4 MΩ when filled with the following standard internal solution (in mM): 126 K Gluconate, 4 NaCl, 1 $MgSO_4$, 0.02 $CaCl_2$, 0.1 BAPTA, 15 Glucose, 5 HEPES, 3 ATP, 0.1 GTP (pH 7.2 with KOH). Passive and active parameters were recorded using an EPC10 USB amplifier (HEKA Elektronik, Reutlingen, Germany) in either voltage-clamp or current-clamp configuration. The resting membrane potential (V_{rest}) was measured after switching to the current-clamp configuration at I = 0 pA. Current-clamp recordings of neuronal firing activity and the following analysis were performed as previously described.[35] Neurons were held at a potential of −70 mV and action potentials (APs) were induced by injection of 10 pA current steps for 1 s. Input resistance (R_{in}) was calculated in the linear region of the voltage–current relationship after the injection of hyperpolarizing and depolarizing current steps (−20, −10, 10, 20 pA). The specific conductance (nS/pF) was obtained by dividing the conductance (R_{in}^{-1}) by the cell capacitance. To study firing activity, the current injection was adjusted to obtain an initial membrane potential of −70 mV before stimulation. The rheobase was calculated as the minimum depolarizing current needed to elicit the first AP. The mean firing frequency was calculated as the ratio between the number of APs evoked by minimal current injection and the time interval (s) between the first and the last evoked AP. To study neuronal stimulation by light-driven glutamate diffusion, APs were recorded from hippocampal neurons plated on top of pSMA-coated Si_3N_4 membrane devices. After glutamate administration (10 mM) *via* an external syringe pump (50 μL min^{-1}, 4 min, Harvard Apparatus) at the bottom side of pSMA-coated Si_3N_4 membrane devices and light stimulation (Lumencor, Inc., Beaverton, OR), APs were recorded by clamping neurons at a holding potential 0 mV in "on-cell" mode for cell-attach configuration. The light stimulation protocol (for both near-UV and white light) was composed of a sequence of 10, 10 and 20 repetitions of a train of 30 light pulses (50 Hz, duty cycle, 50%) interspersed by 600 ms of dark. For near-UV light stimulation, 390 nm light at 100 mW mm^{-2} was used. The combination of 475 nm at 44 mW mm^{-2}, 510 nm at 10 mW mm^{-2}, and 555 nm at 54 mW mm^{-2} was used for the white light stimulation protocol. Data analysis was carried out with custom scripts in MATLAB (*MATLAB Release R2024a*. The MathWorks, Inc., 2024).

Retinal explants and electrophysiological recordings

Royal college of surgeons (RCS) rats, aged 2 months, were dark-adapted for 30 to 60 min prior to the experiments. Following

dark adaptation, rats were euthanized under dim red light using CO_2 inhalation, followed by cervical dislocation. The eyes were then enucleated, and the eyecups were placed in AMES medium (USBiological Life Science, USA) bubbled with a mixture of 5% CO_2 and 95% O_2.

Retinas were carefully dissected from the sclera, cut into quarters, and placed onto the nanodevice, which was mounted on a microfluidic system designed to load compounds into the reservoir in a watertight manner. Retinal pieces were positioned on nanopore arrays with the retinal RGCs facing upwards to facilitate patch-clamp recordings. Whole-cell patch-clamp recordings were obtained from RGCs using an EPC10 amplifier (20 kHz, HEKA Elektronik, Reutlingen, Germany). For current-clamp recordings of retinal explants, borosilicate patch pipettes (with a final resistance of 4.5–6.0 MΩ) were filled with the following solution (in mM): 126 K-gluconate, 4 NaCl, 0.02 $CaCl_2$, 0.1 BAPTA, 0.1 EGTA-KOH, 1 $MgSO_4$, 15 Glucose, 3 ATP-Na2, 0.1 GTP-Na, 5 HEPES, pH 7.3. To study voltage changes after stimulation, the current injection was adjusted to obtain an initial membrane potential of −60 mV. The RGC membrane potential was recorded in the current-clamp configuration, first during a baseline period in the dark, and subsequently during exposure to near-UV (390 nm, 85 mW mm^{-2}) and green (475 nm, 317 mW mm^{-2}) light. Light stimulation was provided by a Spectra X light engine (Lumencor, Inc., Beaverton, OR). Each stimulation protocol, either near-UV or green, consisted of a sequence of trains of 30 light pulses (50 Hz, duty cycle of 50%), followed by 600 ms of darkness. Trains were repeated between 10 and 200 times per sequence, with each sequence being repeated a variable number of times while monitoring RGC firing activity. The acquired signals were then high-pass filtered (cutoff frequency: 100 Hz) and divided into 25-s segments to identify spikes as signal peaks that exceeded 10 times the standard deviation of the 25-s segment. This method was used to minimize the impact of variable and long-term signal noise. The timestamps of detected spikes were subsequently used to generate PSTHs of firing activity (bin size: 30 s). All data analysis was carried out with custom scripts in MATLAB (*MATLAB Release R2024a*. The MathWorks, Inc., 2024).

Ethical approval

All animal procedures were performed in accordance with the National Institutes of Health Guidelines (1996) and the guidelines established by the European Community Council (Directive 2012/63/EU of 22 September 2010) and respective National regulations and authorizations. The study was performed in accordance with Animal Welfare/Ethics Committee (Organismo Preposto al Benessere Animale, OPBA) of the animal facility of the Ospedale Policlinico San Martino (Italian authorization n. 24237 24/06/2021).

Author contributions

MBF fabricated the devices and characterized them with electron microscopy, fabricated the nanovalve devices and studied their optical properties. FT supervised the optical spectroscopy measurements. IP, ABC and PLWW curated the engineering and synthesis of the polymer together with its characterization, while being supervised by JCMH. FV and FG performed the experiments with primary neurons and retinal explants, supervised by SDM. FV and FG performed the cytocompatibility experiments. EC and FB contributed to the supervision of the experiments. FDA and EC conceived the manuscript and coordinated the efforts. MBF, TG, FV, and FG drafted the manuscript that was revised by EC, FB and FDA. All authors have given approval to the final version of the manuscript.

Data availability

The data supporting this article is hosted at the Istituto Italiano di Tecnologia and available in the IIT "gitlab" repository **https://gitlab.iit.it**.

Conflicts of interest

There are no conflicts to declare.

Acknowledgements

The study was supported by EU Horizon 2020 FET Project HyVIS (GA no. 964468 to EC, FDA, and JCMH), Compagnia di S. Paolo Foundation Torino (Project CSPTO 2019.0986 to EC and FDA), Fondazione Roche per la Ricerca Indipendente (2023), and IRCCS Ospedale Policlinico San Martino Genova (Ricerca Corrente and 5 × 1000 grants to FB and EC). We thank Rossana Ciancio, Ilaria Dallorto, Arta Mehilli, Riccardo Navone, and Diego Moruzzo (Istituto Italiano di Tecnologia, Genova, Italy) for technical and administrative assistance. We finally thank Dr A. Toma and Dr M. Leoncini for their support in the clean-room facility.

References

1 K. Sou, D. L. Le and H. Sato, *Small*, 2019, **15**, 1900132.
2 A. Jonsson, T. A. Sjöström, K. Tybrandt, M. Berggren and D. T. Simon, *Sci. Adv.*, 2016, **2**, e1601340.
3 T. A. Sjöström, A. Jonsson, E. O. Gabrielsson, M. Berggren, D. T. Simon and K. Tybrandt, *Adv. Mater. Technol.*, 2020, **5**, 1900750.
4 W. Haq, J. Dietter, S. Bolz and E. Zrenner, *J. Neural Eng.*, 2018, **15**, 45004.
5 V. Monge-Fuentes, A. Biolchi Mayer, M. R. Lima, L. R. Geraldes, L. N. Zanotto, K. G. Moreira, O. P. Martins, H. L. Piva, M. S. S. Felipe and A. C. Amaral, *et al.*, *Sci. Rep.*, 2021, **11**, 15185.
6 C. W. Olanow, P. Calabresi and J. A. Obeso, *Mov. Disord*, 2020, **35**, 1731.
7 R. Liu, R. Zuo and G. A. Hudalla, *Adv. Drug Delivery Rev.*, 2021, **170**, 238.
8 B. P. Timko and D. S. Kohane, *Isr. J. Chem.*, 2013, **53**, 728.

9 O. S. Thomas and W. Weber, *Front. Bioeng. Biotechnol.*, 2019, **7**, 415.
10 M. J. Mitchell, M. M. Billingsley, R. M. Haley, M. E. Wechsler, N. A. Peppas and R. Langer, *Nat. Rev. Drug Discovery*, 2021, **20**, 101.
11 J. Zhang, Y. Lin, Z. Lin, Q. Wei, J. Qian, R. Ruan, X. Jiang, L. Hou, J. Song and J. Ding, *et al.*, *Adv. Sci.*, 2022, **9**, 2103444.
12 D. Wu and Q. Chen, *Signal Transduction Targeted Ther.*, 2023, **8**, 217.
13 C. L. Stevenson, J. T. Santini Jr. and R. Langer, *Adv. Drug Delivery Rev.*, 2012, **64**, 1590.
14 V. Caprettini, A. Cerea, G. Melle, L. Lovato, R. Capozza, J.-A. Huang, F. Tantussi, M. Dipalo and F. De Angelis, *Sci. Rep.*, 2017, **7**, 8524.
15 J. A. Huang and V. Caprettini, *Nano Lett.*, 2019, **19**, 722.
16 S. E. Alavi, S. Alharthi, S. F. Alavi, S. Z. Alavi, G. E. Zahra, A. Raza and H. Ebrahimi Shahmabadi, *Drug Discovery Today*, 2024, **29**, 103936.
17 A. M. Packer, B. Roska and M. Häusser, *Nat. Neurosci.*, 2013, **16**, 805.
18 V. Busskamp and B. Roska, *Curr. Opin. Neurobiol.*, 2011, **21**, 942.
19 K. L. Montgomery, A. J. Yeh, J. S. Ho, V. Tsao and S. Mohan Iyer, *Nat. Methods*, 2015, **12**, 969.
20 M. R. Antognazza, N. Martino, D. Ghezzi, P. Feyen, E. Colombo, D. Endeman, F. Benfenati and G. Lanzani, *Adv. Mater.*, 2015, **27**, 7662.
21 C. M. Rountree, A. Raghunathan, J. B. Troy and L. Saggere, *Microsyst. Nanoeng.*, 2017, **3**, 17052.
22 J. Ma, N. M. Egodawaththa, C. Guruge, O. A. Valladares Márquez, M. Likes and N. Nesnas, *J. Photochem. Photobiol., A*, 2024, **447**, 115183.
23 J. M. Silva, E. Silva and R. L. Reis, *J. Controlled Release*, 2019, **298**, 154.
24 J. Keyvan Rad, Z. Balzade and A. R. Mahdavian, *J. Photochem. Photobiol., C*, 2022, **51**, 100487.
25 M. Ghani, A. Heiskanen, P. Thomsen, M. Alm and J. Emnéus, *ACS Appl. Bio Mater.*, 2021, **4**, 1624.
26 M. Younis, S. Ahmad, A. Atiq, M. Amjad Farooq, M.-H. Huang and M. Abbas, *Chem. Rec.*, 2023, **23**, e202300126.
27 F. Vacca, F. Galluzzi, M. Blanco-Formoso, T. Gianiorio, A. F. De Fazio, F. Tantussi, S. Sturmer, W. Haq, E. Zrenner and A. Chaffiol, *et al.*, *Nano Lett.*, 2024, **24**, 15215–15225.
28 R. Klajn, *Chem. Soc. Rev.*, 2014, **43**, 148.
29 A. Gal, Y. Li, D. A. Thompson, J. Weir, U. Orth, S. G. Jacobson, E. Apfelstedt-Sylla and D. Vollrath, *Nat. Genet.*, 2000, **26**, 270.
30 T. C. Südhof, *Neuron*, 2012, **75**, 11.
31 W. Van der Kloot, *Prog. Neurobiol.*, 1991, **36**, 93.
32 R. Heidelberger, W. B. Thoreson and P. Witkovsky, *Prog. Retinal Eye Res.*, 2005, **24**, 682.
33 H. Wässle, *Nat. Rev. Neurosci.*, 2004, **5**, 747.
34 R. H. Masland, *Neuron*, 2012, **76**, 266.
35 P. Valente, G. Lignani and L. Medrihan, *J. Cell Sci.*, 2016, **129**, 1878.